HHS Public Access

Author manuscript

Nano Lett. Author manuscript; available in PMC 2020 March 06.

Published in final edited form as:

Nano Lett. 2020 February 12; 20(2): 1218–1225. doi:10.1021/acs.nanolett.9b04622.

Differential Charging in Photoemission from Mercurated DNA Monolayers on Ferromagnetic Films

Dominik M. Stemer[1,2], **John M. Abendroth**[1,3], **Kevin M. Cheung**[1,3], **Matthew Ye**[1,3], **Mohammed S. El Hadri**[4], **Eric E. Fullerton**[4], **Paul S. Weiss**[1,2,3,*]

[1]California NanoSystems Institute, University of California, Los Angeles, Los Angeles, California 90095, United States

[2]Department of Materials Science & Engineering, University of California, Los Angeles, Los Angeles, California 90095, United States

[3]Department of Chemistry & Biochemistry, University of California, Los Angeles, Los Angeles, California 90095, United States

[4]Center for Memory and Recording Research, University of California, San Diego, La Jolla, California 92093, United States

Abstract

Spin-dependent and enantioselective electron–molecule scattering occurs in photoelectron transmission through chiral molecular films. This spin selectivity leads to electron spin filtering by molecular helices, with increasing magnitude, concomitant with increasing numbers of helical turns. Using ultraviolet photoelectron spectroscopy, we measured spin-selective surface charging accompanying photoemission from ferromagnetic substrates functionalized with monolayers of mercurated DNA hairpins that constitute only *one* helical turn. Mercury ions bind specifically at thymine–thymine mismatches within self-hybridized single-stranded DNA, enabling precise control over the number and position of Hg^{2+} along the helical axis. Differential charging of the organic layers, manifested as substrate magnetization-dependent photoionization energies, was observed for DNA hairpins containing Hg^{2+}; no differences were measured for hairpin monolayers in the absence of Hg^{2+}. Inversion of the DNA helical secondary structure at increased metal loading led to complementary inversion in spin selectivity. We attribute these results to increased scattering probabilities from relativistic enhancement of spin-orbit interactions in mercurated DNA.

Graphical Abstract

*Corresponding author: psw@cnsi.ucla.edu (PSW).

Author Contributions

The experiments were designed by D.M.S, J.M.A, and P.S.W. Ferromagnetic multilayer substrates with perpendicular magnetic anisotropy were designed and fabricated by M.S.E. and E.E.F. Data were collected by D.M.S., K.M.C., and M.Y. and were analyzed by D.M.S., J.M.A., K.M.C., and P.S.W. Figures were prepared by D.M.S and J.M.A. The manuscript was written by D.M.S., J.M.A., and P.S.W. with assistance from all other authors.

The authors declare no competing financial interests.

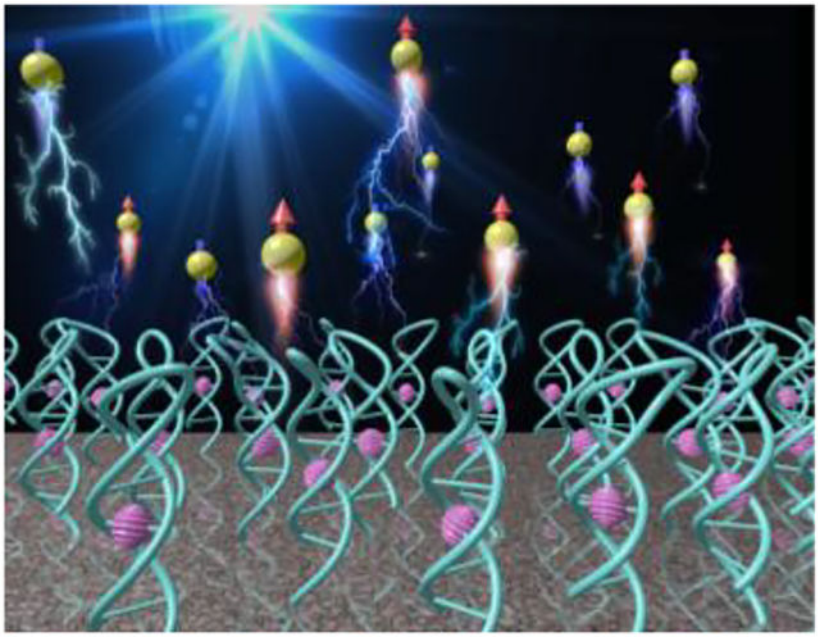

Keywords

Chiral-induced spin selectivity (CISS) effect; electron dichroism; molecular spintronics; photoelectron spectroscopy; DNA nanotechnology

Understanding and controlling enantioselective interactions between chiral molecules and spin-polarized electrons offers exciting opportunities to improve organic spintronic devices,[1–3] photovoltaics,[4,5] enantioseparations,[6,7] and photochemistries.[8,9] These interactions also suggest biological significance due to spin-dependent charge polarization, separation, and recombination experimentally demonstrated at room-temperature within peptides,[10,11] proteins,[12,13] and oligonucleotides,[14,15] and bear possible contributions to the origins of homochirality in Nature.[16,17] Observations of spin-selective electron–chiral molecule interactions, collectively described by the chiral-induced spin selectivity (CISS) effect,[18–20] have been modeled using varying theoretical approaches.[21–24] While it is understood that molecular chirality, time-reversal symmetry breaking, and spin-orbit interactions are required, substantial spin polarization is counterintuitive due to the weak spin-orbit coupling strength of light atoms in organic species (~8 meV for carbon atoms), and thus the weak magnetic field experienced in the rest frame of a moving electron.[25] Possible explanations for which a system can overcome this intrinsic limitation include curvature effects such as in carbon nanotubes, fullerenes, and curved graphene,[26] as well as degeneracy-induced amplification of spin-orbit perturbations.[27]

Still, unified mechanisms remain elusive. Moreover, unambiguous determination of spin-dependent scattering asymmetries with diamagnetic molecules can be experimentally difficult under ambient conditions. Early investigations into spin-dependent interactions between electrons and chiral species stemmed from efforts in enantioselective synthesis or decomposition of optical isomers using circularly polarized light.[28] Mirroring possible

sources of circularly polarized light in Nature, experiments that utilized radioactive isotopes that undergo β-decay as light sources to generate *bremsstrahlung* from the deceleration of β-particles led to emergent hypotheses that polarized electrons themselves interacted selectively with left- or right-handed molecules.[29,30] However, challenged by the small degree of spin polarization observed in electron scattering from optically active molecules, subsequent experiments designed to test these spin-dependent interactions led to mixed results.[31–36]

To amplify possible electron dichroic effects,[37] Mayer and Kessler tested for asymmetry in scattering by D- and L-camphor derivatives containing high atomic number (Z) atoms with anticipated increased spin-orbit interactions between electrons and gas-phase chiral molecules.[38–40] In these experiments, while neither transmission asymmetry nor chirality-induced spin polarization of polarized electron beams through vapors of unmodified camphor were observed, electron dichroism was measured for vapors of camphor-lanthanoid complexes. Asymmetry was observed to increase roughly with the atomic number of the metal atom, as Pr (Z = 59) < Eu (Z = 63) ~ Er (Z = 68) < Yb (Z = 70). In more recent studies of spin-selective electron transmission through chiral vapors of bromo- and iodo-camphor, Gay and coworkers have also reported Z-dependent scattering asymmetries. However, it has proven difficult to deconvolute intertwined causal parameters, including spin-orbit effects, atomic proximity to a chiral center, and electron helicity density within the molecule itself.[41–43]

Göhler and coworkers later measured room-temperature spin filtering in photoemission from Au substrates functionalized with self-assembled monolayers (SAMs) of double-stranded DNA with spin polarization of ~60% for photoelectrons transmitted through helices constituting eight helical turns (78 base pairs).[44] This strong spin polarization was attributed to the higher density and more uniform orientation of helical molecules in films compared to dilute molecular vapors.[45,46] Importantly, asymmetric scattering probabilities have been shown to depend on electron kinetic energies; the de Broglie wavelength of photoelectrons must be commensurate with the length of the molecular helices,[47] suggesting lower likelihood of spin selectivity in photoemission for low kinetic energy electrons transmitted through short DNA strands (*i.e.*, one to two helical turns). However, incorporation of high-Z species into the helical framework should enhance the scattering rate *via* relativistic effects, thus amplifying asymmetry induced by the chiral environment.

Herein, we apply ultraviolet photoelectron spectroscopy (UPS) to probe spin selectivity in photoemission from SAMs of right- and left-handed DNA hairpins composed of only *ca.* one helical turn with *vs* without divalent Hg (Z = 80) ions bound along the molecular axis (Figure 1). We recently demonstrated the use of this technique to measure magnetization-dependent photoemission from chiral molecular films composed of α-helical peptides and globular proteins assembled on ferromagnetic multilayer (FM) substrates in the kinetic energy range of *ca.* 0–18 eV.[48] In these studies, spectra were collected using a He I source with photon energy high enough (21.22 eV) to ionize the DNA films assembled on FM substrates. Because the radiation was not circularly polarized, direct photoionization of the molecules should not depend on molecular handedness.[49] However, photoelectrons emitted from the underlying ferromagnetic substrate with sufficient kinetic energy can ionize the

overlying molecules by electron impact.[50] The polarization of photoelectrons emitted from the underlying ferromagnetic film nominally reflects the film's magnetization orientation (parallel *vs* antiparallel to surface normal). In this context, differential charging of the organic films between substrate magnetization orientations, physically manifested as differences in photoionization energies, is indicative of spin-dependent electron ionization cross sections.

Stoichiometric equivalents of Hg^{2+} were coordinated precisely at thymine–thymine (T-T) mismatches in DNA, stabilizing hybridized strands *via* metal-mediated base pairing (Figure 2a–c).[51–57] The manner of metal incorporation and coordination depend on the character of the metal. In the presence of T-T mismatches, Hg^{2+} exhibits linear coordination, forming bonds 2–3 times stronger than those of typical hydrogen-bonded base pairs.[58] The coordination of Hg^{2+} within DNA containing T-T mismatches is highly specific, enabling control over the density and position of Hg^{2+} within each self-hybridized DNA hairpin by varying the number and position of T-T mismatches in a given sequence.

To track DNA structural changes upon mercuration, we characterized Hg^{2+} binding in sequences with zero, one, two, three, and seven T-T mismatches, hereafter referred to as 0MM, 1MM, 2MM, 3MM, and 7MM, respectively (Figures 2 and S2). The 0MM sequence, composed of (5'→3') TTT GTA AGA AGG CCC CCC TTC TTA CAA A, where G is guanine, A is adenine, and C is cytosine, enables self-hybridization due to complementarity between 12 base pairs, promoting hairpin formation with a single-stranded loop. Increasing the number of base-pair mismatches by replacing A with T subsequently destabilizes hairpin formation. However, this stability is recovered upon incubation with $Hg(NO_3)_2$ as indicated by melting curve analyses in the presence and absence of stoichiometric equivalents of Hg^{2+} (Figures 2d–f, S2c,d).

Increasing absorbance at 260 nm with increasing temperature is characteristic of a denaturing transition. For 0MM DNA in 1× phosphate-buffered saline (PBS), no changes in melting temperature (T_M) of the hairpins were observed upon addition of one molar equivalent of Hg^{2+} (Figure 2d), suggesting that any possible electrostatic binding of Hg^{2+} with the negatively charged backbone of DNA does not affect the stability of the molecule. For 1MM DNA, a T_M increase of ~7°C upon addition of one equivalent of Hg^{2+} was measured, indicating increased stability of the hairpin due to the formation of coordinate covalent metal-base bonds at T-T sites (Figure 2e).[52,54,56] Melting curves collected for 2MM and 3MM DNA showed larger increases in T_M when compared to their unmercurated counterparts (Figure S2c,d). For 7MM DNA, no clear temperature-dependent melting transition was observed between 25°C and 85°C, either in the presence or absence of Hg^{2+} (Figure 2f), suggesting an ill-defined solution-phase melting point below room temperature, likely caused by the high proportion of T-T mismatches as a percentage of total nucleotide content.

Complementary structural characterization of all sequences in the presence and absence of stoichiometric $Hg(NO_3)_2$ in 1× PBS was carried out using circular dichroism (CD) spectroscopy to probe the relationship between increasing incorporation of Hg^{2+} and the helical secondary structure of the DNA, depending on the number of T-T mismatches

present in the sequence. Distinct bisignate peaks, characteristic of B-form variants of DNA duplexes, were observed between 240 and 280 nm for 0MM, suggesting the formation of right-handed DNA hairpins. The CD spectra for 0MM did not change upon addition of 1 molar equivalent of $Hg(NO_3)_2$, providing further evidence that possible non-specific electrostatic interactions between Hg^{2+} and the DNA backbone do not disrupt secondary structure (Figure 2g). The 1MM sequence exhibited a slight decrease in peak intensity at 280 nm upon Hg^{2+} addition (Figure 2h),[59] while the 2MM and 3MM sequences exhibited further secondary structural changes (Figure S2g,f), as evidenced by the increasing attenuation of signal intensity at 280 nm. In the most pronounced case, the long-wavelength peak near 280 nm exhibited almost complete inversion for 7MM, signaling a complementary inversion of secondary structure, from a right-handed to left-handed helical conformation (Figure 2i). This behavior has been observed previously in mercurated hairpins with many T-T mismatches.[52,60–62]

Self-assembled monolayers of 0MM, 1MM, and 7MM were prepared on FM substrates with perpendicular magnetic anisotropy, composed of glass substrate/Ta (3 nm)/Pt (2 nm)/$[Co (0.6 nm)/Pt (0.3 nm)]_{69}$/Co (0.6 nm)/Au (2 nm), both in the presence and absence of stoichiometric $Hg(NO_3)_2$. The Au capping layer enabled formation of Au–S bonds between the substrate and the molecules for self-assembly of the thiol-modified oligonucleotides. Further, oligonucleotide SAMs were backfilled with 6-mercapto-1-hexanoic acid to promote orientations of the hairpins nominally normal to the substrate surfaces.[63–65] Substrates were magnetized to saturation either “up” (magnetization orientation parallel to surface normal) or “down” (antiparallel) prior to SAM formation. The presence of mercury on sample surfaces following DNA SAM formation was confirmed *via* X-ray photoelectron spectroscopy (XPS) only for monolayers composed of 1MM and 7MM (Figure S3).

Analyses of UPS spectra were conducted for substrates magnetized up *vs* down for each experimental condition. Film photoionization energies, I, were calculated as:

$$I = h\nu - (E_B^{max} - E_B^{min}) = h\nu - W \quad (1)$$

where $h\nu$ is the photon energy, E_B^{max} is the maximum binding energy at the secondary electron cutoff, E_B^{min} is the energy at the valence band edge, and W is the spectral width. Magnified spectral regions of E_B^{max} and E_B^{min} are shown for representative samples in Figure 3a–d.

No dependence of I on substrate magnetization orientation was measured for SAMs of 0MM (Figure 3e). This was expected, considering that these DNA hairpins were composed of only 12 hybridized bases (Figure 2a), and therefore likely support too few helical turns to allow for detectable spin-selective effects.[44,47] The measured values of I for SAMs of 1MM with and without Hg^{2+} are presented in Figure 3f. Differences in ionization energy between 0MM and 1MM samples were attributed to nucleobase substitution; adenine has a lower ionization energy than thymine, in DNA.[66.67] The association of nucleobases into hydrogen-bonded or metal-mediated base pairs is accompanied by further reductions in ionization energy.[55,68] Two-way analysis of variance (ANOVA) revealed significant dependence of the preferred

substrate magnetization orientation on DNA/Hg^{2+} film composition (Table S1; $P < 0.05$). Subsequent *post hoc* tests revealed significant differences in I only for 1MM SAMs prepared in the presence of Hg^{2+}. Higher I, and therefore greater buildup of positive charge in the organic film, was measured for 1MM SAMs when substrates were magnetized up, compared to down. The 0MM and 1MM SAMs consist of nearly identical DNA sequences, with comparable secondary structures, only differing in the presence or absence of a single mercurated base pair. Thus, these data indicate that the spin-dependent asymmetry in the photoelectron–chiral molecule interaction cross section is enhanced due to higher scattering rates *via* the heavy atom effect.

In contrast, lower I was measured for substrates magnetized up *vs* down functionalized with SAMs composed of 7MM DNA with Hg^{2+} (Figure 3g). The inverted magnetization orientation dependence of I for SAMs of mercurated 7MM DNA compared with SAMs of mercurated 1MM DNA correlates with the opposite handedness of their secondary structures (left-handed for 7MM and right-handed for 1MM) as indicated by CD spectroscopy (Figure 2h,j). The chiral electrostatic field experienced by an electron interacting with a molecular helix is dependent on the handedness of arrangement of atoms in the molecule. Reversal in molecular handedness is expected to be accompanied by a concomitant reversal in spin dependence for electron scattering interactions accompanying transmission through chiral films in photoemission. These experimental results agree qualitatively with the helicity-dependent DNA-mediated charge transport demonstrated by Zwang *et al.* in electrochemical studies, and with measurements of opposite spin polarization of photoelectrons emitted from noble metal substrates functionalized with (*M*)- and (*P*)-heptahelicene.[15,46]

Interestingly, despite the higher surface density of heavy ion scattering centers for SAMs composed of mercurated 7MM *vs* 1MM, the absolute magnitude differences in I between magnetization up and down conditions (−37 meV and 51 meV, respectively) were comparable in both sets of measurements. Previous measurements by Nolting *et al.* of scattering asymmetry by spin-polarized electron beams through vapors of singly *vs* doubly brominated camphor derivatives analogously showed no obvious enhancement in asymmetry by increasing the number of heavy atoms in each molecule. In fact, the absolute maximum scattering asymmetries were slightly larger for bromocamphor than for dibromocamphor.[40] Similarly, in our experiments, spin selectivity in electron–chiral molecule interactions for DNA hairpins containing multiple heavy atoms may experience compensating, rather than amplifying, effects. However, due to the poorly defined thermal stability of 7MM at room temperature, as well as the incomplete reversal from right-handed to left-handed secondary structure in the presence of Hg^{2+}, we note that the spin-selective ionization energy asymmetry measured herein may not represent the maximum obtainable with a heavily mercurated sequence of this length.

The magnetic dipole moment of an electron lies antiparallel to its spin angular momentum; within a ferromagnetic material, the spin angular momentum of an electron within the majority subband is oriented antiparallel to the net magnetization direction of the material. We note that for SAMs formed of mercurated right-handed 1MM DNA, the measured ionization energies were lower when the substrates were magnetized down, corresponding to a lower ionization cross section for photoelectrons with right-handed helicity (spin parallel

to velocity). When compared to previous reports of preferential transmission of photoelectrons with left-handed helicity through right-handed chiral molecules without metal ion inclusions,[45] these results indicate that additional mechanisms may be involved in metallized systems.

The sign and magnitude of the electric dipole across a molecule adsorbed on a substrate affect the work function of that material; a dipole pointing toward the surface induces a work function increase, while a dipole pointing away from the surface lowers the work function of the sample.[69,70] In molecules lacking strong internal dipoles (along the axis parallel to the surface normal), the net dipole moment is dominated by that of the Au-thiol bond, which decreases the work function of the surface.[71–73] We note that FM substrates functionalized with 1MM had higher work functions than those functionalized with 1MM + Hg^{2+}, independent of magnetization conditions (Figure S4). However, both of these samples exhibited lower work functions than the analogous bare substrates measured previously.[48] This work function decrease indicates that the addition of Hg^{2+} reinforces the intrinsic dipole of the molecule, rather than compensating or reversing it. Additionally, it is possible that the magnetic characteristics of the heavy ions are capable of influencing the spin-dependent interaction cross section asymmetry. Here, we have investigated Hg^{2+}, a diamagnetic ion. Further studies comparing paramagnetic to diamagnetic inclusions, as well as stringently controlling the location of incorporated metal ions along the helical axis, should elucidate any effects introduced by intrinsic ion magnetization or molecular dipole augmentation.

In conclusion, we report spin-selective interaction asymmetries between photoelectrons and DNA molecules assembled on perpendicularly-magnetized ferromagnetic multilayer substrates, manifest as differential charging by molecular ionization from inelastic scattering of spin-polarized photoelectrons. Substrate magnetization-dependent photoionization energies in DNA assemblies were only observed when Hg^{2+} ions were bound at T-T mismatches within the DNA hairpins. We attribute the results to increased spin-orbit interactions in electron scattering by DNA due to the presence of the heavy metal species. The substrate magnetization-dependent effects were reversed between right-handed and left-handed helical hairpins, as expected for spin-dependent and enantioselective interactions between electrons and chiral molecules. Incorporation of high-Z metals into chiral molecular scaffolds may prove a practical means to systematically elucidate molecular and environmental parameters in a predictive way by amplifying spin-selective interaction asymmetries. If heavy-metallization of chiral molecular species also enables tuning and enhancing the chiral-induced spin selectivity effect in the conduction regime, length limitations of helical molecules for strong spin polarization in transport may be averted, benefiting miniaturization in the development organic-based spintronic devices and detectors.[19]

Supplementary Material

Refer to Web version on PubMed Central for supplementary material.

ACKNOWLEDGMENTS

We gratefully acknowledge National Science Foundation ECCS Grant #1509794 for support of this work. K.M.C. and P.S.W. also thank the National Institute on Drug Abuse (DA045550) for support. Work at UCSD was supported by National Science Foundation DMR Grant #1610538. The authors acknowledge the use of instruments at the Nano and Pico Characterization Lab at the California NanoSystems Institute, and the UCLA Molecular Instrumentation Center. We would like to thank Dr. Ignacio Martini Laboratory for helpful discussions regarding UPS and Chuanzhen Zhao for assistance with figure illustration.

REFERENCES

(1). Varade V; Markus TZ; Vankayala K; Friedman N; Sheves M; Waldeck DH; Naaman R Bacteriorhodopsin Based Non-Magnetic Spin Filters for Biomolecular Spintronics. Phys. Chem. Chem. Phys 2017, 20, 1091–1097.

(2). Koplovitz G; Primc D; Ben Dor O; Yochelis S; Rotem D; Porath D; Paltiel Y Magnetic Memory: Magnetic Nanoplatelet-Based Spin Memory Device Operating at Ambient Temperatures. Adv. Mater 2017, 29, 1606748.

(3). Al-Bustami H; Koplovitz G; Primc D; Yochelis S; Capua E; Porath D; Naaman R; Paltiel Y Single Nanoparticle Magnetic Spin Memristor. Small 2018, 14, 1–6.

(4). Peer N; Dujovne I; Yochelis S; Paltiel Y Nanoscale Charge Separation Using Chiral Molecules. ACS Photonics 2015, 2, 1476–1481.

(5). Purcell-Milton F; McKenna R; Brennan LJ; Cullen CP; Guillemeney L; Tepliakov NV; Baimuratov AS; Rukhlenko ID; Perova TS; Duesberg GS; Baranov AV; Fedorov AV; Gun'ko YK Induction of Chirality in Two-Dimensional Nanomaterials: Chiral 2D MoS_2 Nanostructures. ACS Nano 2018, 12, 954–964. [PubMed: 29338193]

(6). Banerjee-Ghosh K; Dor O. Ben; Tassinari F; Capua E; Yochelis S; Capua A; Yang SH; Parkin SSP; Sarkar S; Kronik L; Baczewski LT; Naaman R; Paltiel Y Separation of Enantiomers by Their Enantiospecific Interaction with Achiral Magnetic Substrates. Science 2018, 360, 1331–1334. [PubMed: 29748324]

(7). Tassinari F; Steidel J; Paltiel S; Fontanesi C; Lahav M; Paltiel Y; Naaman R Enantioseparation by Crystallization Using Magnetic Substrates. Chem. Sci 2019, 10, 5246–5250. [PubMed: 31191879]

(8). Mtangi W; Kiran V; Fontanesi C; Naaman R Role of the Electron Spin Polarization in Water Splitting. J. Phys. Chem. Lett 2015, 6, 4916–4922. [PubMed: 26615833]

(9). Ghosh KB; Zhang W; Tassinari F; Mastai Y; Lidor-Shalev O; Naaman R; Möllers P; Nürenberg D; Zacharias H; Wei J; Wierzbinski E; Waldeck DH Controlling Chemical Selectivity in Electrocatalysis with Chiral CuO-Coated Electrodes. J. Phys. Chem. C 2019, 123, 3024–3031.

(10). Kumar A; Capua E; Kesharwani MK; Martin JML; Sitbon E; Waldeck DH; Naaman R Chirality-Induced Spin Polarization Places Symmetry Constraints on Biomolecular Interactions. Proc. Natl. Acad. Sci 2017, 114, 2474–2478. [PubMed: 28228525]

(11). Kettner M; Göhler B; Zacharias H; Mishra D; Kiran V; Naaman R; Fontanesi C; Waldeck DH; Sek S; Pawowski J; Juhaniewicz J Spin Filtering in Electron Transport through Chiral Oligopeptides. J. Phys. Chem. C 2015, 119, 14542–14547.

(12). Carmeli I; Kumar KS; Heifler O; Carmeli C; Naaman R Spin Selectivity in Electron Transfer in Photosystem I. Angew. Chemie - Int. Ed 2014, 53, 8953–8958.

(13). Roy P; Kantor-uriel N; Mishra D; Dutta S; Friedman N; Sheves M; Naaman R Spin-Controlled Photoluminescence in Hybrid Nanoparticles Purple Membrane System. ACS Nano 2016, 10, 4525–4531. [PubMed: 27018195]

(14). Abendroth JM; Nakatsuka N; Ye M; Kim D; Fullerton EE; Andrews AM; Weiss PS Analyzing Spin Selectivity in DNA-Mediated Charge Transfer *via* Fluorescence Microscopy. ACS Nano 2017, 11, 7516–7526. [PubMed: 28672111]

(15). Zwang TJ; Hürlimann S; Hill MG; Barton JK Helix-Dependent Spin Filtering through the DNA Duplex. J. Am. Chem. Soc 2016, 138, 15551–15554. [PubMed: 27934017]

(16). Rosenberg RA Electrochirogenesis: The Possible Role of Low-Energy Spin-Polarized Electrons in Creating Homochirality. Symmetry 2019, 11, 528.

(17). Michaeli K; Kantor-Uriel N; Naaman R; Waldeck DH The Electron's Spin and Molecular Chirality-How Are They Related and How Do They Affect Life Processes? Chem. Soc. Rev 2016, 45, 6478–6487. [PubMed: 27734046]

(18). Naaman R; Waldeck DH Chiral-Induced Spin Selectivity Effect. J. Phys. Chem. Lett 2012, 3, 2178–2187. [PubMed: 26295768]

(19). Abendroth JM; Stemer DM; Bloom BP; Roy P; Naaman R; Waldeck DH; Weiss PS; Mondal PC Spin Selectivity in Photoinduced Charge Transfer Mediated by Chiral Molecules. ACS Nano 2019, 13, 4928–4946. [PubMed: 31016968]

(20). Naaman R; Paltiel Y; Waldeck DH Chiral Molecules and the Electron Spin. Nat. Rev. Chem 2019, 3, 250–260.

(21). Díaz E; Domínguez-Adame F; Gutierrez R; Cuniberti G; Mujica V Thermal Decoherence and Disorder Effects on Chiral-Induced Spin Selectivity. J. Phys. Chem. Lett 2018, 9, 5753–5758. [PubMed: 30212207]

(22). Gutierrez R; Díaz E; Gaul C; Brumme T; Domínguez-Adame F; Cuniberti G Modeling Spin Transport in Helical Fields: Derivation of an Effective Low-Dimensional Hamiltonian. J. Phys. Chem. C 2013, 117, 22276–22284.

(23). Gutierrez R; Díaz E; Naaman R; Cuniberti G Spin-Selective Transport through Helical Molecular Systems. Phys. Rev. B - Condens. Matter Mater. Phys 2012, 85, 081404.

(24). Matityahu S; Utsumi Y; Aharony A; Entin-Wohlman O; Balseiro CA Spin-Dependent Transport through a Chiral Molecule in the Presence of Spin-Orbit Interaction and Nonunitary Effects. Phys. Rev. B 2016, 93, 1–12.

(25). National Institute of Standards and Technology. Atomic Spectra Database. http://www.nist.gov/pml/atomic-spectra-database (accessed Aug 27, 2019).

(26). Huertas-Hernando D; Guinea F; Brataas A Spin-Orbit Coupling in Curved Graphene, Fullerenes, Nanotubes, and Nanotube Caps. Phys. Rev. B - Condens. Matter Mater. Phys 2006, 74, 155426.

(27). Dalum S; Hedegård P Theory of Chiral Induced Spin Selectivity. Nano Lett. 2019, 19, 5253–5259. [PubMed: 31265313]

(28). Ulbricht TLV Asymmetry: The Non-Conservation of Parity and Optical Activity. Q. Rev 1959, 13, 48–60.

(29). Ulbricht TLV; Vester F Attempts to Induce Optical Activity with Polarized β–Radiation. Tetrahedron 1962, 18, 629–637.

(30). Garay AS Origin and Role of Optical Isomery in Life. Nature 1968, 219, 338–340. [PubMed: 5662146]

(31). Keszthelyi L Origin of the Asymmetry of Biomolecules and Weak Interaction. Orig. Life 1977, 8, 299–340. [PubMed: 611424]

(32). Hodge LA; Dunning FB; Walters GK; White RH; Shroepfer GJ Degradation of DL-Leucine with Longitudinally Polarised Electrons. Nature 1979, 280, 250–252.

(33). Beerlage MJM; Farago PS; Van Der Wiel MJ Search for Spin Effects in Low-Energy Electron Scattering from Optically Active Camphor. J. Phys. B At. Mol. Phys 1981, 14, 3245–3253.

(34). Campbell DM, Farago PS Spin-Dependent Electron Scattering from Optically Active Molecules. Nature 1985, 317, 52–53.

(35). Campbell D; Farago PJ Electron Optic Dichroism in Camphor. Phys. Chem. B 1987, 20, 5133.

(36). Fandreyer R; Thompson D; Blum K Attenuation of Longitudinally Polarized Electron Beams by Chiral Molecules. J. Phys. B At. Mol. Opt. Phys 1990, 23, 3031–3040.

(37). Blum K; Thompson D Spin-Dependent Electron Scattering from Oriented Molecules. J. Phys. B At. Mol. Opt. Phys 1989, 22, 1823–1844.

(38). Mayer S; Kessler J Experimental Verification of Electron Optic Dichroism. Phys. Rev. Lett 1995, 74, 4803–4806. [PubMed: 10058603]

(39). Mayer S; Nolting C; Kessler J Electron Scattering from Chiral Molecules. J. Phys. Chem. Lett 1996, 29, 3497–3511.

(40). Nolting C; Mayer S; Kessler J Electron Dichroism - New Data and an Experimental Cross-Check. J. Phys. B At. Mol. Opt. Phys 1997, 30, 5491–5499.

(41). Scheer AM; Gallup GA; Gay TJ An Investigation of Electron Helicity Density in Bromocamphor and Dibromocamphor as a Source of Electron Circular Dichroism. J. Phys. B At. Mol. Opt. Phys 2006, 39, 2169–2181.

(42). Dreiling JM; Lewis FW; Mills JD; Gay TJ Anomalously Large Chiral Sensitivity in the Dissociative Electron Attachment of 10-Iodocamphor. Phys. Rev. Lett 2016, 116, 1–5.

(43). Dreiling JM; Lewis FW; Gay TJ Spin-Polarized Electron Transmission through Chiral Halocamphor Molecules. J. Phys. B At. Mol. Opt. Phys 2018, 51.

(44). Göhler B; Hamelbeck V; Markus TZ; Kettner M; Hanne GF; Vager Z; Naaman R; Zacharias H Spin Selectivity in Electron Transmission through Self-Assembled Monolayer of Double-Stranded DNA. Science 2011, 331, 894–897. [PubMed: 21330541]

(45). Ray K; Ananthavel SP; Waldeck DH; Naaman R Asymmetric Scattering of Polarized Electrons by Organized Organic Films of Chiral Molecules. Science 1999, 283, 814–816. [PubMed: 9933157]

(46). Kettner M; Maslyuk VV; Nürenberg D; Seibel J; Gutierrez R; Cuniberti G; Ernst K-H; Zacharias H Chirality-Dependent Electron Spin Filtering by Molecular Monolayers of Helicenes. J. Phys. Chem. Lett 2018, 9, 2025–2030. [PubMed: 29618210]

(47). Rosenberg RA; Symonds JM; Kalyanaraman V; Markus T; Orlando TM; Naaman R; Medina EA; Lo FA; Mujica V Kinetic Energy Dependence of Spin Filtering of Electrons Transmitted through Organized Layers of DNA. J. Phys. Chem. C 2013, 117, 22307–22313.

(48). Abendroth JM; Cheung KM; Stemer DM; El Hadri MS; Zhao C; Fullerton EE; Weiss PS Spin-Dependent Ionization of Chiral Molecular Films. J. Am. Chem. Soc 2019, 141, 3863–3874. [PubMed: 30734553]

(49). Heinzmann U; Schönhense G; Kessler J Polarization of Photoelectrons Ejected by Unpolarized Light from Xenon Atoms. Phys. Rev. Lett 1979, 42, 1603–1605.

(50). Kisker E; Gudat W; Schröder K Observation of a High Spin Polarization of Secondary Electrons from Single Crystal Fe and Co. Solid State Commun. 1982, 44, 591–595.

(51). FrØystein NA; Sletten E Interaction of Mercury(II) with the DNA Dodecamer CGCGAATTCGCG. A ^{1}H and ^{15}N NMR Study. J. Am. Chem. Soc 1994, 116, 3240–3250.

(52). Miyake Y; Togashi H; Tashiro M; Yamaguchi H; Oda S; Kudo M; Tanaka Y; Kondo Y; Sawa R; Fujimoto T; Machinami T; Ono A Mercury^{II}-Mediated Formation of Thymine-Hg^{II}-Thymine Base Pairs in DNA Duplexes. J. Am. Chem. Soc 2006, 128, 2172–2173. [PubMed: 16478145]

(53). Tanaka Y; Oda S; Yamaguchi H; Kondo Y; Kojima C; Ono A ^{15}N-^{15}N J-Coupling across Hg^{II}: Direct Observation of Hg^{II}-Mediated T-T Base Pairs in a DNA Duplex. J. Am. Chem. Soc 2007, 129, 244–245. [PubMed: 17212382]

(54). Torigoe H; Ono A; Kozasa T Hg^{II} Ion Specifically Binds with T:T Mismatched Base Pair in Duplex DNA. Chem. - A Eur. J 2010, 16, 13218–13225.

(55). Miyachi H; Matsui T; Shigeta Y; Hirao K Effects of Mercury(II) on Structural Properties, Electronic Structure and UV Absorption Spectra of a Duplex Containing Thymine-Mercury(II)-Thymine Nucleobase Pairs. Phys. Chem. Chem. Phys 2010, 12, 909–917. [PubMed: 20066376]

(56). Yamaguchi H; Šebera J; Kondo J; Oda S; Komuro T; Kawamura T; Dairaku T; Kondo Y; Okamoto I; Ono A; Burda JV; Kojima C; Sychrovsky V; Tanaka Y The Structure of Metallo-DNA with Consecutive Thymine-Hg^{II}-Thymine Base Pairs Explains Positive Entropy for the Metallo Base Pair Formation. Nucleic Acids Res. 2014, 42, 4094–4099. [PubMed: 24371287]

(57). Kondo J; Yamada T; Hirose C; Okamoto I; Tanaka Y; Ono A Crystal Structure of Metallo DNA Duplex Containing Consecutive Watson-Crick-like T-Hg^{II}-T Base Pairs. Angew. Chemie - Int. Ed 2014, 53, 2385–2388.

(58). Takezawa Y; Shionoya M Metal-Mediated DNA Base Pairing: Alternatives to Hydrogen-Bonded Watson-Crick Base Pairs. Acc. Chem. Res 2012, 45, 2066–2076. [PubMed: 22452649]

(59). Kypr J; Kejnovská I; Renčiuk D; Vorlícková M Circular Dichroism and Conformational Polymorphism of DNA. Nucleic Acids Res. 2009, 37, 1713–1725. [PubMed: 19190094]

(60). Walter A; Luck G Interactions of Hg(II) Ions with DNA as Revealed by CD Measurements. Nucleic Acids Res. 1977, 4, 539–550. [PubMed: 559300]

(61). Gruenwedel DW; Cruikshank MK Mercury-Induced Transitions between Right-Handed and Putative Left-Handed Forms of Poly[d(A-T) d(A-T)] and Poly[d(G-C) d(G–C)]. Nucleic Acids Res. 1989, 17, 9075–9086. [PubMed: 2555784]

(62). Gruenwedel DW; Cruikshank MK Mercury-Induced DNA Polymorphism: Probing the Conformation of Hg(II)-DNA *via* Staphylococcal Nuclease Digestion and Circular Dichroism Measurements. Biochemistry 1990, 29, 2110–2116. [PubMed: 2328243]

(63). Lee CY; Gong P; Harbers GM; Grainger DW; Castner DG; Gamble LJ Surface Coverage and Structure of Mixed DNA/Alkylthiol Monolayers on Gold: Characterization by XPS, NEXAFS, and Fluorescence Intensity Measurements. Anal. Chem 2006, 78, 3316–3325. [PubMed: 16689532]

(64). Josephs EA; Ye T Nanoscale Spatial Distribution of Thiolated DNA on Model Nucleic Acid Sensor Surfaces. ACS Nano 2013, 7, 3653–3660. [PubMed: 23540444]

(65). Cao HH; Nakatsuka N; Serino AC; Liao WS; Cheunkar S; Yang H; Weiss PS; Andrews AM Controlled DNA Patterning by Chemical Lift-Off Lithography: Matrix Matters. ACS Nano 2015, 9, 11439–11454. [PubMed: 26426585]

(66). Belau L; Wilson KR; Leone SR; Ahmed M Vacuum-Ultraviolet Photoionization Studies of the Microhydration of DNA Bases (Guanine, Cytosine, Adenine and Thymine). J. Phys. Chem. A 2007, 111, 7562–7568. [PubMed: 17419600]

(67). Bravaya KB; Kostko O; Dolgikh S; Landau A; Ahmed M; Krylov AI Electronic Structure and Spectroscopy of Nucleic Acid Bases: Ionization Energies, Ionization-Induced Structural Changes, and Photoelectron Spectra. J. Phys. Chem. A 2010, 114, 12305–12317. [PubMed: 21038927]

(68). Rooman M; Wintjens R Sequence and Conformation Effects on Ionization Potential and Charge Distribution of Homo-Nucleobase Stacks Using M06–2X Hybrid Density Functional Theory Calculations. J. Biomol. Struct. Dyn 2014, 32, 532–545. [PubMed: 23582046]

(69). Kim J; Rim YS; Liu Y; Serino AC; Thomas JC; Chen H; Yang Y; Weiss PS Interface Control in Organic Electronics Using Mixed Monolayers of Carboranethiol Isomers. Nano Lett. 2014, 14, 2946–2951. [PubMed: 24773449]

(70). Serino AC; Anderson ME; Saleh LMA; Dziedzic RM; Mills H; Heidenreich LK; Spokoyny AM; Weiss PS Work Function Control of Germanium through Carborane-Carboxylic Acid Surface Passivation. ACS Appl. Mater. Interfaces 2017, 9 (40), 34592–34596. [PubMed: 28920673]

(71). De Renzi V; Rousseau R; Marchetto D; Biagi R; Scandolo S; Del Pennino U Metal Work-Function Changes Induced by Organic Adsorbates: A Combined Experimental and Theoretical Study. Phys. Rev. Lett 2005, 95, 3–6.

(72). De Boer B; Hadipour A; Mandoc MM; Van Woudenbergh T; Blom PWM Tuning of Metal Work Functions with Self-Assembled Monolayers. Adv. Mater 2005, 17, 621–625.

(73). Alloway DM; Graham AL; Yang X; Mudalige A; Colorado R; Wysocki VH; Pemberton JE; Lee TR; Wysocki RJ; Armstrong NR Tuning the Effective Work Function of Gold and Silver Using ω-Functionalized Alkanethiols: Varying Surface Composition through Dilution and Choice of Terminal Groups. J. Phys. Chem. C 2009, 113, 20328–20334.

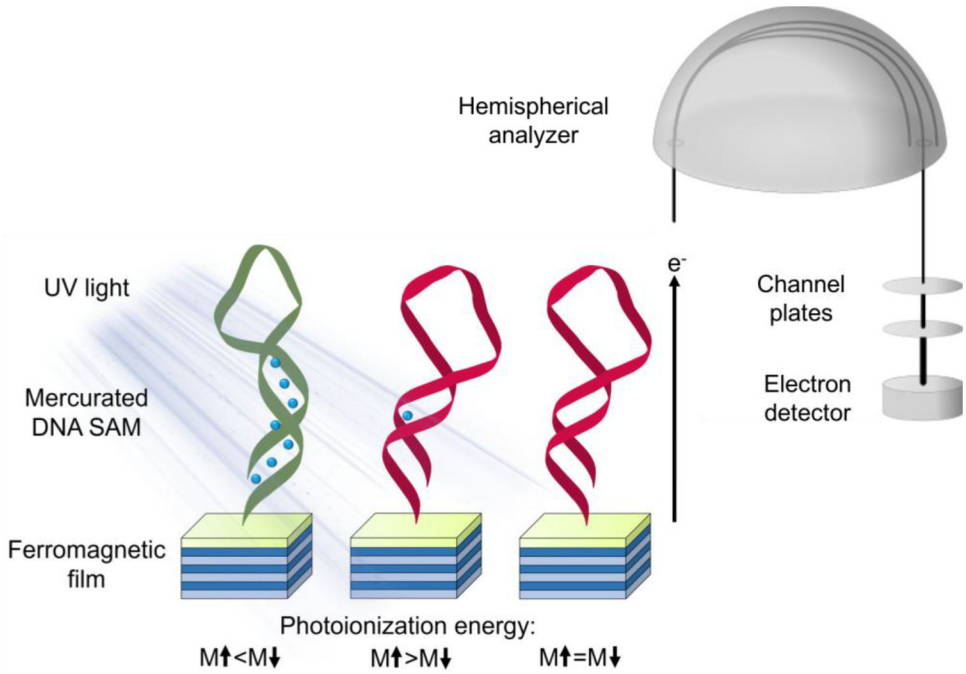

Figure 1.

Experimental schematic illustrating photoemission from ferromagnetic surfaces functionalized with left- (green) or right-handed (red) DNA hairpins containing divalent mercury ions. Photoelectrons emitted from magnetized substrates undergo spin-selective scattering cross-sections with the DNA molecules due to the chiral-induced spin selectivity effect. Ionizing collisions due to spin-up vs spin-down photoelectrons of sufficient energy with DNA lead to differential charging, manifested as substrate magnetization (M)-dependent photoionization energies.

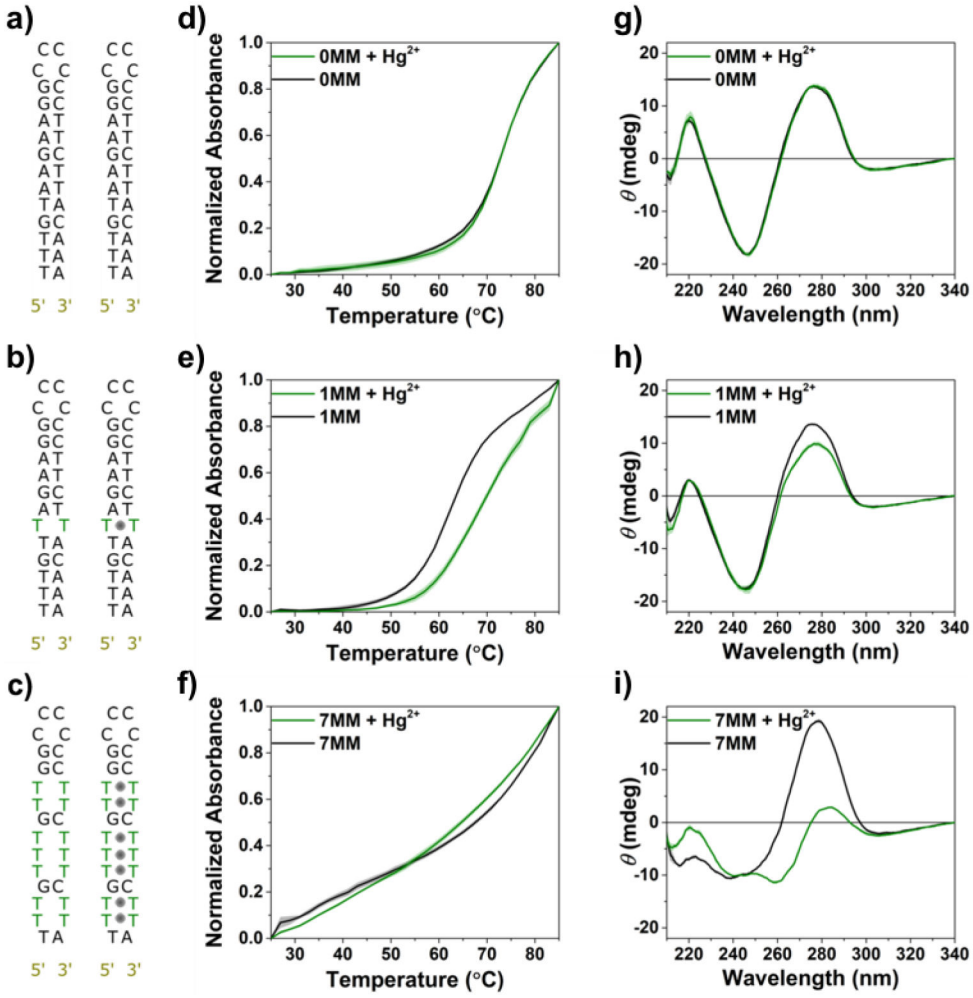

Figure 2.

a-c) Schematics of DNA with 0 thymine-thymine mismatches (0MM), 1MM, and 7MM, respectively, illustrating number of thymine-thymine mismatches (left), and of the same sequences in the presence of Hg^{2+} ions (represented as solid grey circles). **d-f)** Melting curves for 0MM, 1MM, and 7MM. Peak absorbance at 260 nm is normalized to the maximum value for each curve. **g-i)** Circular dichroism spectra for 0MM, 1MM, and 7MM. Melting curves and circular dichroism were collected for each sequence in the presence (green) or absence (black) of stochiometric Hg^{2+}. The concentration of all DNA solutions was 5 μM. Shaded areas represent standard errors of the mean (N = 3).

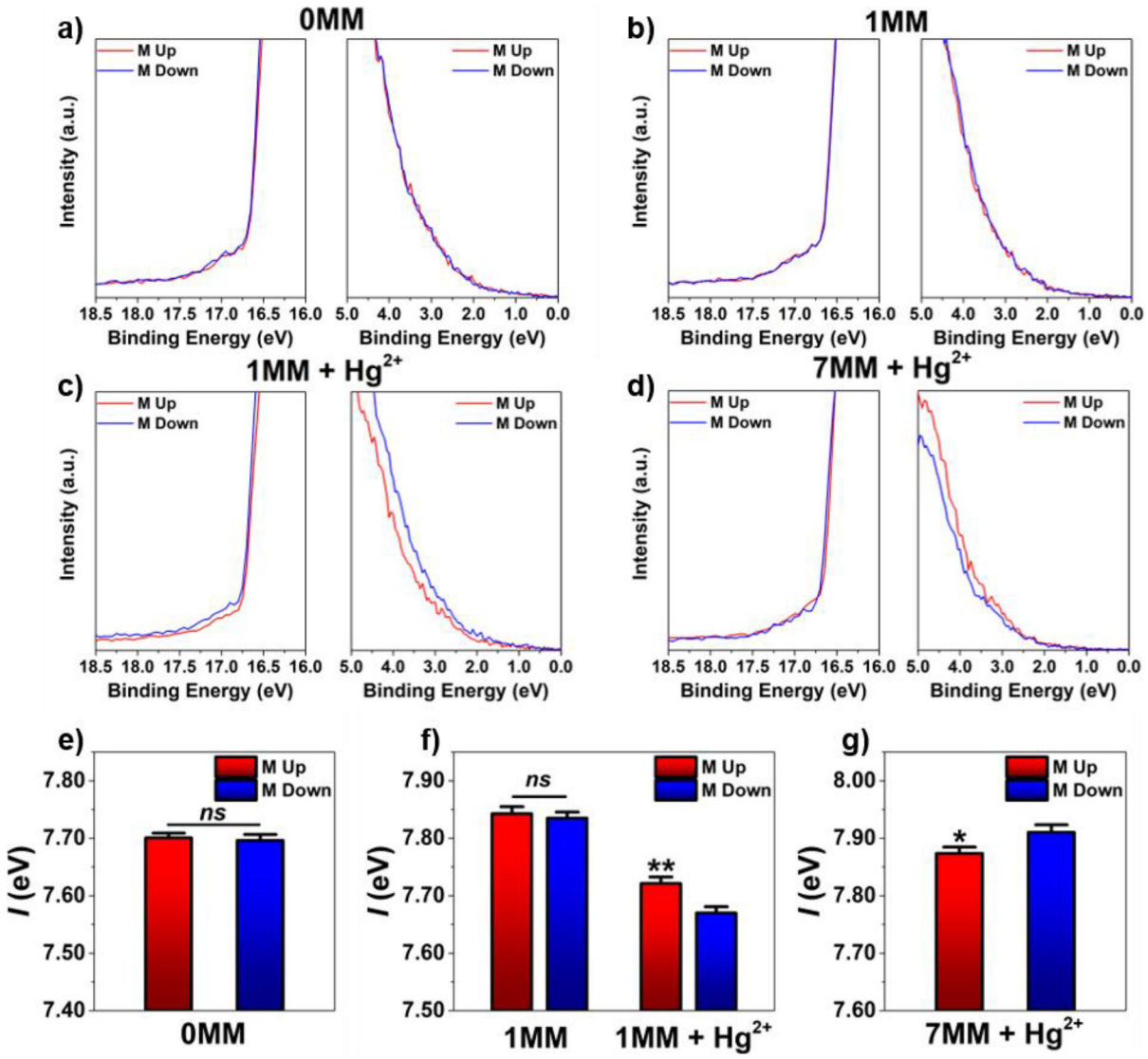

Figure 3.

a-d) Representative secondary electron cutoff (left) and Fermi edge (right) for DNA with 0 thymine-thymine mismatches (0MM), 1MM, 1MM + Hg^{2+}, and 7MM + Hg^{2+}, respectively. Photoionization energies collected under field up (red) and down (blue) substrate saturation magnetization conditions for self-assembled monolayers of **e)** 0MM, **f)** 1MM & 1MM + Hg^{2+}, and **g)** 7MM + Hg^{2+}. Error bars represent standard error of the mean. Number of samples (N) = 19 [0MM Up], 19 [0MM Down], 20 [1MM Up], 20 [1MM Down], 20 [1MM + Hg^{2+} Up], 20 [1MM + Hg^{2+} Down], 19 [7MM + Hg^{2+} Up], and 20 [7MM + Hg^{2+} Down]. *$P < 0.05$ *vs* M down; **$P < 0.01$ *vs* M down; *ns* = not significant.